Emergent Defect States as a Source of Resistivity Anisotropy in the Nematic Phase of Iron Pnictides

Maria N. Gastiasoro,[1] I. Paul,[2] Y. Wang,[3] P. J. Hirschfeld,[3] and Brian M. Andersen[1]
[1]*Niels Bohr Institute, University of Copenhagen, Universitetsparken 5, DK-2100 Copenhagen, Denmark*
[2]*Laboratoire Matériaux et Phénomènes Quantiques (UMR 7162 CNRS), Université Paris Diderot-Paris 7, Bâtiment Condorcet, 75205 Paris Cedex 13, France*
[3]*Department of Physics, University of Florida, Gainesville, Florida 32611, USA*
(Received 1 July 2014; published 15 September 2014)

We consider the role of potential scatterers in the nematic phase of Fe-based superconductors above the transition temperature to the $(\pi, 0)$ magnetic state but below the orthorhombic structural transition. The anisotropic spin fluctuations in this region can be frozen by disorder, to create elongated magnetic droplets whose anisotropy grows as the magnetic transition is approached. Such states act as strong anisotropic defect potentials that scatter with much higher probability perpendicular to their length than parallel, although the actual crystal symmetry breaking is tiny. We calculate the scattering potentials, relaxation rates, and conductivity in this region and show that such emergent defect states are essential for the transport anisotropy observed in experiments.

DOI: 10.1103/PhysRevLett.113.127001 PACS numbers: 74.70.Xa, 72.10.Fk, 74.62.En

The origin of electronic nematic behavior, i.e., spontaneous breaking of discrete rotational symmetry preserving translational symmetry, is one of the most fascinating questions in the field of Fe-based superconductivity, involving the interplay of magnetic, orbital, and ionic fluctuations. Strong in-plane anisotropy has been reported in transport [1–7], angular resolved photoemission [8], neutron scattering [9], optical spectroscopy [10,11], and torque magnetometry [12] measurements. Since the various fluctuation channels in these multiband systems all couple below the tetragonal to orthorhombic structural transition at T_s in many systems, all response functions become anisotropic and it is not easy to decide which fluctuations drive the ordering nematic phenomena observed. Theoretically, both spin nematic and orbital scenarios have been proposed [13].

In systems with large spin nematic susceptibility, strong anisotropy is expected in the spin fluctuations in the orthorhombic phase below T_s, even if the structural anisotropy is small. Such anisotropy will certainly influence transport properties; this is the basis of theories of transport by several groups [14–16], arguing that at T_s the magnetic correlation length becomes anisotropic and drives the anisotropy in the electronic inelastic scattering rate. Disorder is described through a momentum-independent scattering rate and is required only to limit the contribution to the resistivity anisotropy from "cold spots" on the Fermi surface. The transport anisotropy has also been recently studied within numerical Monte Carlo simulations of the spin-fermion model [17].

In this work, the transport anisotropy of the nematic phase is also explained via spin fluctuation anisotropy, but through the generation of strongly anisotropic impurity states. Our work is motivated by the observation by many STM experiments of C_4 symmetry breaking around point defects locally [18–24]; these experiments can exhibit effects that are missed by average bulk probes. In fact, in some systems evidence for nematic symmetry breaking in the form of highly anisotropic C_2 defect states is seen in the nominally tetragonal phase above T_s [24]. These responses are generally attributed to residual local strains that break C_4 symmetry locally, together with a large residual nematic susceptibility [25]. In the ordered stripe $(\pi, 0)$ magnetic phase below the Néel temperature T_N, the C_4 symmetry is broken by the magnetism itself. Nevertheless, the symmetry breaking of the electronic structure around local Co defects in lightly doped Ca122 was observed to be so enhanced that this result was cited as the first evidence for a strong nematic tendency in these systems [18]. In addition, as suggested in Ref. [23], such "nematogen" defects could be responsible for the transport anisotropy.

Recently, we examined the microscopic origin of nematic defect states in the ordered phase and proposed that they result from the effect of a nonmagnetic impurity on the energy balance between two magnetic phases, the $(\pi, 0)$ stripe ground state and a nearby (π, π) competing Néel state [26]. The relative stability of the latter at hole doping leads to an elongated dimerlike structure in both charge distribution and low-energy LDOS in agreement with experiments [18,23]. C_4-broken impurity states were discussed earlier in the context of localized spin models [27] and pinned fluctuating orbital order [28,29], but in neither case was the dimerlike structure seen in experiment reported.

The emergent nematogen defect states found in Ref. [26] become C_4 symmetric above T_N in the tetragonal phase. Yet transport anisotropy experiments in Ba122 exhibit

significant anisotropy also in the "nematic phase" $T_N < T < T_s$, where there is no long-range magnetic stripe order, or in the tetragonal phase in the presence of external stress [1–7]. It is not clear, however, whether nematogens can form around pointlike impurities in this phase, i.e., whether the anisotropic spin fluctuations in a spin-nematic scenario can condense around a defect to give a similar transport anisotropy in this case.

There are several key aspects of the transport experiments [1–7] above T_N that any theory needs to account for. These are (1) the counterintuitive sign of the resistivity anisotropy on the electron-doped side, where $\rho_b > \rho_a$ although $b < a$, (2) the decrease of the anisotropy upon annealing [6], (3) the pronounced increase in ρ_b as T_N is approached, with continued metallicklike behavior of ρ_a, (4) the decrease in anisotropy both with increasing T and electron overdoping, and (5) the possible sign change but also significant decrease of the anisotropy on the hole-doped side [5]. We believe that theories that propose transport anisotropy due to scattering of electrons from spin fluctuations alone are able to account for only some of these salient features and that including the role of emergent defect states in these correlated systems provides a more natural explanation for the observations.

In this work, we discuss first the growth of anisotropic spin fluctuations in the nematic phase as T_N is approached from above. We extend the theory of impurity-induced emergent defects states into the nematic phase with an unbiased microscopic calculation of the local electronic structure near a pointlike nonmagnetic impurity potential in a situation where the C_4 symmetry of the host bands has been broken very slightly below T_s. This gives rise to the *same* anisotropic spin fluctuations considered as the source of transport anisotropy by the authors of Refs. [14–16], but strong impurities play a very different and essential role. We find that the impurity state in the nematic phase is strongly anisotropic due to the enhanced background nematic response arising from electronic correlations [30]. Specifically, we calculate the momentum-dependent effective impurity potential, scattering rate, and conductivity in the nematic phase.

The Hamiltonian is given by $\mathcal{H} = \mathcal{H}_0 + \mathcal{H}_{oo} + \mathcal{H}_{\rm int} + \mathcal{H}_{\rm imp}$, where $\mathcal{H}_0$ denotes the kinetic energy

$$\mathcal{H}_0 = \sum_{\mathbf{ij},\mu\nu,\sigma} t^{\mu\nu}_{\mathbf{ij}} c^\dagger_{\mathbf{i}\mu\sigma} c_{\mathbf{j}\nu\sigma} - \mu_0 \sum_{\mathbf{i}\mu\sigma} n_{\mathbf{i}\mu\sigma}, \tag{1}$$

with tight-binding parameters adopted from Ref. [32]. Here, $\mathbf{i}$ and $\mathbf{j}$ denote lattice sites, σ the spin, and μ_0 is the chemical potential that sets the doping level $x = 0$. The indices μ and ν are the five iron d orbitals. $\mathcal{H}_{oo} = \delta/2\sum_{\mathbf{i}}(n_{\mathbf{i}yz} - n_{\mathbf{i}xz})$ mimics the orthorhombicity of the band below T_s, for a nonzero δ orbital splitting. We have also studied C_2 symmetric bands arising from hopping anisotropy and found similar results to those reported below. The interaction term $\mathcal{H}_{\rm int}$ is

$$\mathcal{H}_{\rm int} = U\sum_{\mathbf{i},\mu} n_{\mathbf{i}\mu\uparrow} n_{\mathbf{i}\mu\downarrow} + \left(U' - \frac{J}{2}\right) \sum_{\mathbf{i},\mu<\nu,\sigma\sigma'} n_{\mathbf{i}\mu\sigma} n_{\mathbf{i}\nu\sigma'} - 2J \sum_{\mathbf{i},\mu<\nu} \vec{S}_{\mathbf{i}\mu} \cdot \vec{S}_{\mathbf{i}\nu} + J' \sum_{\mathbf{i},\mu<\nu,\sigma} c^\dagger_{\mathbf{i}\mu\sigma} c^\dagger_{\mathbf{i}\mu\bar{\sigma}} c_{\mathbf{i}\nu\bar{\sigma}} c_{\mathbf{i}\nu\sigma}, \tag{2}$$

including the intraorbital (interorbital) on-site repulsion U (U'), the Hund's coupling J, and the pair hopping energy J'. We assume spin rotation invariance $U' = U - 2J$ and $J' = J$ and fix $U = 1.0$ eV and $J = U/4$. Finally, $\mathcal{H}_{\rm imp} = V_{\rm imp}\sum_{\mu\sigma} c^\dagger_{\mathbf{i}^*\mu\sigma} c_{\mathbf{i}^*\mu\sigma}$ is the impurity potential with $V_{\rm imp} = 1.5$ eV at the impurity site $\mathbf{i}^*$. The particular values for U (and J) and $V_{\rm imp}$ are not important except that both have to be in the range where magnetization is nucleated locally [26]. After mean-field decoupling of Eq. (2), we solve the eigenvalue problem $\sum_{\mathbf{j}\nu} H^{\mu\nu}_{\mathbf{ij}\sigma} u^n_{\mathbf{j}\nu\sigma} = E_{n\sigma} u^n_{\mathbf{i}\mu\sigma}$, where

$$H^{\mu\nu}_{\mathbf{ij}\sigma} = t^{\mu\nu}_{\mathbf{ij}} + \delta_{\mathbf{ij}}\delta_{\mu\nu}[-\mu_0 + \delta(\delta_{\mu yz} - \delta_{\mu xz}) + \delta_{\mathbf{ii}^*} V_{\rm imp} + U\langle n_{\mathbf{i}\mu\bar{\sigma}}\rangle + \sum_{\mu'\neq\mu} (U'\langle n_{\mathbf{i}\mu'\bar{\sigma}}\rangle + (U' - J)\langle n_{\mathbf{i}\mu'\sigma}\rangle)], \tag{3}$$

on a 30×30 lattice with self-consistently obtained densities $\langle n_{\mathbf{i}\mu\sigma}\rangle = \sum_n |u^n_{\mathbf{i}\mu\sigma}|^2 f(E_{n\sigma})$ for each site and orbital.

In the homogeneous orthorhombic nematic phase above T_N, the important effect of the xz-yz orbital splitting is to enhance (diminish) the spin susceptibility at $\mathbf{Q_1} \equiv (\pi, 0)$ [$\mathbf{Q_2} \equiv (0, \pi)$] as shown in Fig. 1 for two cases with $\delta_1 = 16$ meV ($T_N^{\delta_1}$) and $\delta_2 = 80$ meV ($T_N^{\delta_2}$). The enhanced susceptibility at $\mathbf{Q_1} \equiv (\pi, 0)$ pushes T_N up. As seen explicitly from Fig. 1, even a small orbital splitting δ leads eventually to an arbitrarily large spin anisotropy upon

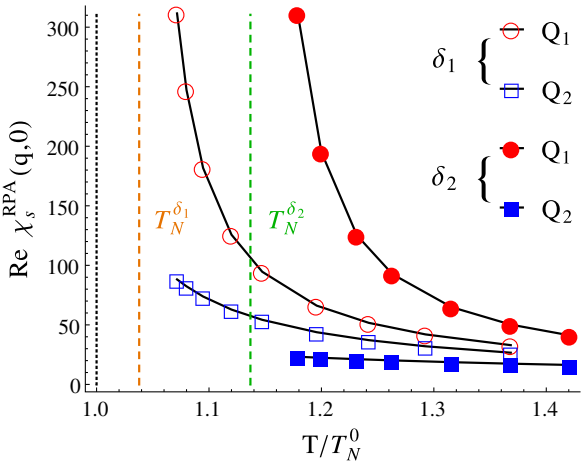

FIG. 1 (color online). Real part of the homogeneous RPA spin susceptibility $\chi_s^{\rm RPA}(\mathbf{q}, 0)$ at $\mathbf{Q_1} \equiv (\pi, 0)$ (red circles) and $\mathbf{Q_2} \equiv (0, \pi)$ (blue squares) as a function of T normalized to the Néel temperature T_N^0 of the tetragonal band ($\delta = 0$). Open (solid) symbols refer to the degree of orbital order, $\delta_1 = 16$ meV ($\delta_2 = 80$ meV), and the dashed green (dashed orange) vertical lines indicate the corresponding relevant T_N^δ.

approaching the instability [30], in agreement with recent neutron scattering measurements [31].

How does the electronic structure near the impurities reflect the spin anisotropy of the nematic phase? In Fig. 2 we show local magnetization $m(\mathbf{r})$ nucleated by an impurity in the nematic state as a function of T. As seen, the emergent defect object pins the order locally [33,34] and therefore incorporates the growing spin fluctuation anisotropy in the host upon approaching the magnetic instability. The growing x-y anisotropy is clearly evident in the Fourier images in the lower row of Fig. 2. These impurity nematogens are the nematic phase equivalents of the nematogens studied below T_N in Ref. [26].

In order to determine the contribution to transport properties of the nematic defect states, we calculate first the scattering rate in the Born approximation

$$\frac{1}{\tau^{l}_{\mathbf{k}\alpha}} = n_{\mathrm{imp}} \frac{2\pi}{\hbar} \frac{1}{V} \sum_{\mathbf{k}'\beta} |\mathrm{tr}[\hat{\sigma}_l \hat{\mathcal{V}}^{\mathrm{imp}}_{\sigma\sigma'}(\mathbf{k}\alpha, \mathbf{k}'\beta)]|^2 \times \delta(\epsilon_{\mathbf{k}\alpha} - \epsilon_{\mathbf{k}'\beta}) \left(1 - \frac{\mathbf{v}^{\alpha}_F(\mathbf{k}) \cdot \mathbf{v}^{\beta}_F(\mathbf{k}')}{|\mathbf{v}^{\alpha}_F(\mathbf{k})||\mathbf{v}^{\beta}_F(\mathbf{k}')|}\right), \quad (4)$$

where $l = 0$ ($l = 3$) corresponds to the charge (magnetic) scattering rate and $1/\tau_{\mathbf{k}\alpha} \equiv 1/\tau^{0}_{\mathbf{k}\alpha} + 1/\tau^{3}_{\mathbf{k}\alpha}$ is the total scattering rate on band α. The term $\hat{\mathcal{V}}^{\mathrm{imp}}_{\sigma\sigma'}(\mathbf{k}\alpha, \mathbf{k}'\beta) \equiv \langle \mathbf{k}'\beta\sigma'|\mathcal{V}^{\mathrm{imp}}|\mathbf{k}\alpha\sigma\rangle \equiv \langle \mathbf{k}'\beta\sigma'|\mathcal{H} - \mathcal{H}_{(V_{\mathrm{imp}}=0)}|\mathbf{k}\alpha\sigma\rangle$ is the matrix element of the impurity Hamiltonian for the fully converged self-consistent eigenvalue problem

$$\hat{\mathcal{V}}^{\mathrm{imp}}_{\sigma\sigma'}(\mathbf{k}\alpha, \mathbf{k}'\beta) = \sum_{\mu\nu} a^{\alpha*}_{\mathbf{k}\mu} \omega^{\mu\nu}_{\mathbf{k}\sigma\mathbf{k}'\sigma'} a^{\beta}_{\mathbf{k}'\nu} - \epsilon_{\mathbf{k}\alpha}\delta_{\mathbf{k}\mathbf{k}'}\delta_{\alpha\beta}. \quad (5)$$

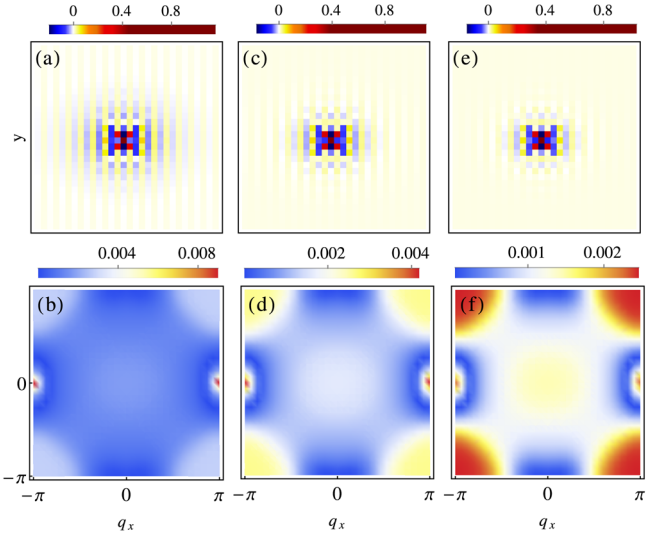

FIG. 2 (color online). Real space magnetization $m(\mathbf{r})$ of a $V_{\mathrm{imp}} = 1.5$ eV impurity for $\delta_2 = 80$ meV at temperatures $T/T_N^{\delta_2} = 1.06$ (a), 1.14 (c), and 1.23 (e). Panels (b), (d), and (f) show the Fourier transform $|m(\mathbf{q})|$ of (a), (c), and (e), respectively.

Here, $\omega^{\mu\nu}_{\mathbf{k}\sigma\mathbf{k}'\sigma'} = 1/N \sum_n \sum_{\mathbf{ij}} u^{n*}_{\mathbf{j}\nu\sigma'} u^{n}_{\mathbf{i}\mu\sigma} E_{n\sigma} e^{-i\mathbf{k}'\mathbf{r}_{\mathbf{j}}} e^{i\mathbf{k}\mathbf{r}_{\mathbf{i}}}$, and $a^{\alpha}_{\mathbf{k}\mu}$ are the matrix elements of the unitary transformation from orbitals to bands. Finally, $\mathbf{v}^{\alpha}_F(\mathbf{k})$ denotes the Fermi velocity of band α, and the last term in parentheses in Eq. (4) is an approximation to the vertex corrections in the full Kubo formula by Ziman [35] that has proven accurate for anisotropic scatterers [36].

In Fig. 3, we show the effect of local freezing of the spin fluctuations on the scattering rate anisotropy by plotting $1/\tau_{\mathbf{k}\alpha}$ explicitly, first for a pointlike scatterer of potential V_{imp} with no self-consistency in Fig. 3(a). It is seen that the distribution of scattering weight reflects the small orbital ordering that has created a slightly orthorhombic Fermi surface. Since V_{imp} is momentum independent, the variation reflects primarily the band-orbital matrix elements for this model. Figure 3(b) now shows how the nematogen scattering rate reflects the intrinsic spin fluctuations in the system. The localized object in real space couples fluctuations at all $\mathbf{q}$, but these include important contributions from those scattering processes that dominate the fluctuations in the homogeneous system, i.e., the scattering between like orbitals on hole and electron pockets as seen in Fig. 3(b). The pointlike scatterer leads to a scattering rate that is nearly T independent, while the nematogen scattering rate grows as the magnetic transition is approached, as

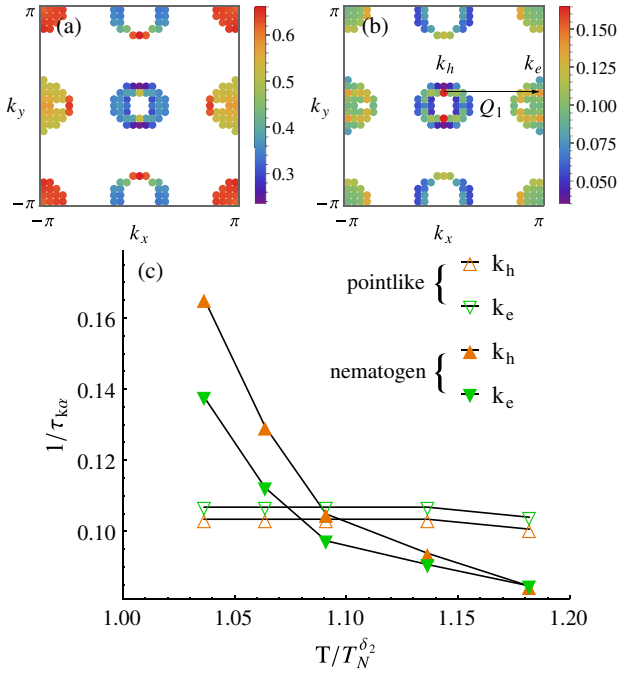

FIG. 3 (color online). (a) Map of $1/\tau_{\mathbf{k}\alpha}$ vs k_x, k_y for pointlike $\hat{\mathcal{V}}^{\mathrm{imp}}_{\sigma\sigma'}(\mathbf{k}\alpha, \mathbf{k}'\beta) = \hat{\sigma}_0 V_{\mathrm{imp}} \sum_{\mu} a^{\alpha*}_{\mathbf{k}\mu} a^{\beta}_{\mathbf{k}'\mu}$ at $T/T_N^{\delta_2} = 1.036$. Values are shown for all $\mathbf{k}$ within a range $\sim 2k_BT$ of the Fermi surface. (b) Same map for nematogen with $\hat{\mathcal{V}}^{\mathrm{imp}}_{\sigma\sigma'}(\mathbf{k}\alpha, \mathbf{k}'\beta)$ determined self-consistently. The arrow indicates the dominant $\mathbf{Q_1}$ scattering between the particle and hole pockets. (c) Scattering rates from (a) (scaled by 1/5) and (b) at $\mathbf{k}_h$, $\mathbf{k}_e$ vs T.

shown in Fig. 3(c). For the nematogen scattering, the charge scattering rate is also nearly T independent. It is the magnetic scattering rate that provides both the strong T dependence and the enhanced anisotropy.

Turning finally to the conductivity obtained from

$$\sigma_{ij} = e^2 \frac{1}{V} \sum_{\mathbf{k}\alpha} \mathrm{v}_i^\alpha(\mathbf{k}) \mathrm{v}_j^\alpha(\mathbf{k}) \tau(\epsilon_{\mathbf{k}\alpha}) \left(-\frac{\partial f}{\partial \epsilon_{\mathbf{k}\alpha}} \right), \quad (6)$$

we show in Fig. 4 the resistivity anisotropy $\Delta\rho = (\rho_b - \rho_a)/\rho_0$ as a function of T with $\rho_0 = (\rho_a + \rho_b)/2$. As expected from Fig. 3, the anisotropy in the case of pointlike scatterers is essentially T independent and caused only by the band, in agreement with Ref. [37].

On the other hand, for the nematogens $\Delta\rho$ rises rapidly upon approaching the magnetic instability, in agreement with experiments. As T_N is approached, the divergence of the spin fluctuation scattering rate is cut off eventually: in our simulation by the system size, in the real sample by the internematogen distance.

With the above results in hand, we can explain the transport properties (1)–(5) discussed in the introduction. The impurity-based scenario with nematogens oriented along the a axis naturally explains points (1) ($\rho_b > \rho_a$) and (2) (annealing dependence). The T dependence of the nematogen scattering rate presented in Fig. 3 explains the upturn in ρ_b upon approaching T_N [point (3)]. Our picture assumes additionally that Ba122, in particular, contains significant amounts of disorder, which determines the large value of the resistivity near T_N. This is consistent with the large constant $\rho(T_N)$ and small T^2 coefficient in the parent and lightly doped materials [6]. These weak scatterers do not pin low-energy spin fluctuations, and hence cannot contribute to the resistivity anisotropy. In the parent compound even after annealing, a few vacancies in the FeAs plane creating stronger scatterers remain and give rise to a small peak in the b-axis resistivity above T_N due to nematogen formation. Upon doping with Co the concentration of nematogens rises quasilinearly, enhances the resistivity anisotropy, and leads to peaks in ρ_b, as seen in experiment, until the critical doping where T_N goes to zero and the spin fluctuations driving the anisotropy weaken [point (4)]. Hole doping with K, on the other hand, introduces much weaker out-of-plane scatterers that cannot induce nematogens [26]; the anisotropy is then essentially zero, with the exception of that driven by few residual vacancies [point (5)]. We have checked that within our model the sign of the anisotropy indeed changes on the hole-doped side as in experiment, but this is a band-structure effect; the more important property is the dramatic collapse of the anisotropy also observed in the hole-doped system [5].

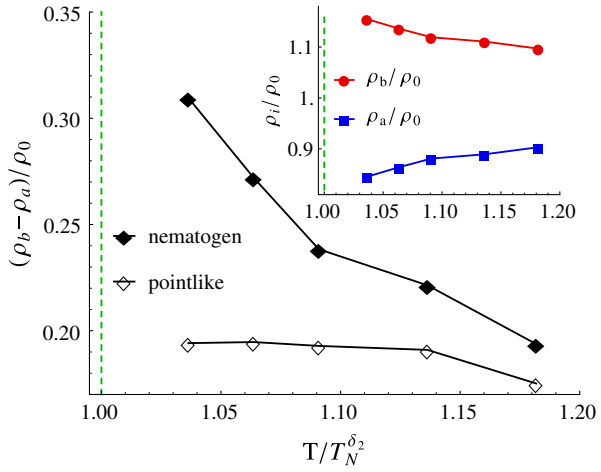

FIG. 4 (color online). Resistivity anisotropy $\Delta\rho$ vs T for non-self-consistent pointlike (open diamonds) and self-consistent nematogen (filled diamonds) impurity scatterers. Inset shows the T dependence of ρ_a/ρ_0 (circles) and ρ_b/ρ_0 (squares) for the nematogen case.

We emphasize again that the physics of resistivity anisotropy in our view arises ultimately from the same anisotropy in the spin fluctuation spectrum invoked by the authors of Refs. [14–16]. Nevertheless, the importance of these fluctuations in the current picture is that they condense into an emergent defect state above T_N whose anisotropy grows in response to the small orthorhombic symmetry breaking below T_s, which then scatters electrons anisotropically. We have shown that a tiny Fermi surface asymmetry, reflected in a very weak anisotropy of the Drude weight [38], is dramatically enhanced by spin fluctuations near T_N such that scattering rate anisotropies of order 100% are possible.

Strong evidence in favor of this picture comes from the annealing experiments of Ishida *et al.* [6], who show that when strong disorder is removed, the anisotropy drops, and attribute the remaining anisotropy to Co atoms, as we do here. While a reduction in anisotropy with decreasing disorder is also possible in the inelastic scattering models, as pointed out, e.g., by Breitkreiz *et al.* [16], it occurs in a parameter regime where spin fluctuation scattering dominates elastic scattering, in contrast to the situation in experiments.

While these theories account for the dramatic reduction of anisotropy on the hole-doped side, this agreement depends on the ellipticity of the 2D electron bands assumed. In the Ba122 system, however, the electron pockets have an ellipticity that changes sign with k_z, leading to a near cancellation of band-structure contributions to the anisotropy. The scattering rate anisotropy due to the nematogens, on the other hand, depends uniquely on the orthorhombicity, rather than special features of the band. We note that the nematic susceptibility measured in this material is quite electron-hole symmetric [39].

Recently, Kuo and Fisher [7] criticized the idea of an extrinsic source of the anisotropy, since samples with very different residual resistivity ratios have similar resistivity anisotropies, and different chemical substituents corresponding to the same doping exhibit similar anisotropies

as well. Neither of these observations contradicts our analysis, however, since, first, the large differences in sample quality and residual resistivity ratio are caused largely by out-of-plane disorder that does not create nematogens. Second, for potentials strong enough to create nematogens, the anisotropy in the scattering rate arises from the spin fluctuations themselves; the strength of the potential for different impurities affects mainly the magnitude of the average resistivity and much less its anisotropy.

In summary, we have discussed an impurity-driven scenario for the remarkable transport anisotropy in Fe-based superconductors that explains all essential features of these measurements and argues for an increased focus on the unusual role played by impurities in these systems with strong spin fluctuations near a magnetic transition.

We thank M. Breitkreiz, R. M. Fernandes, and C. Timm for discussions. B. M. A. and M. N. G. acknowledge support from Lundbeckfond fellowship (Grant No. A9318). P. J. H. and Y. W. were supported by NSF-DMR-1005625.

[1] M. A. Tanatar, E. C. Blomberg, A. Kreyssig, M. G. Kim, N. Ni, A. Thaler, S. L. Budko, P. C. Canfield, A. I. Goldman, I. I. Mazin, and R. Prozorov, Phys. Rev. B **81**, 184508 (2010).
[2] J.-H. Chu, J. G. Analytis, K. De Greve, P. L. McMahon, Z. Islam, Y. Yamamoto, and I. R. Fisher, Science **329**, 824 (2010).
[3] J. J. Ying, X. F. Wang, T. Wu, Z. J. Xiang, R. H. Liu, Y. J. Yan, A. F. Wang, M. Zhang, G. J. Ye, P. Cheng, J. P. Hu, and X. H. Chen, Phys. Rev. Lett. **107**, 067001 (2011).
[4] J.-H. Chu, H.-H. Kuo, J. G. Analytis, and I. R. Fisher, Science **337**, 710 (2012).
[5] E. C. Blomberg, M. A. Tanatar, R. M. Fernandes, I. I. Mazin, B. Shen, H.-H. Wen, M. D. Johannes, J. Schmalian, and R. Prozorov, Nat. Commun. **4**, 1914 (2013).
[6] S. Ishida, M. Nakajima, T. Liang, K. Kihou, C. H. Lee, A. Iyo, H. Eisaki, T. Kakeshita, Y. Tomioka, T. Ito, and S. Uchida, Phys. Rev. Lett. **110**, 207001 (2013); J. Am. Chem. Soc. **135**, 3158 (2013).
[7] H.-H. Kuo and I. R. Fisher, Phys. Rev. Lett. **112**, 227001 (2014).
[8] M. Yi, D. Lu, J.-H. Chu, J. G. Analytis, A. P. Sorini, A. F. Kemper, B. Moritz, S.-K. Mo, R. G. Moore, M. Hashimoto, W.-S. Lee, Z. Hussain, T. P. Devereaux, I. R. Fisher, and Z.-X. Shen, Proc. Natl. Acad. Sci. U.S.A. **108**, 6878 (2011).
[9] J. Zhao, D. T. Adroja, D.-X. Yao, R. Bewley, S. Li, X. F. Wang, G. Wu, X. H. Chen, J. Hu, and P. Dai, Nat. Phys. **5**, 555 (2009).
[10] M. Nakajima, S. Ishida, Y. Tomioka, K. Kihou, C. H. Lee, A. Iyo, T. Ito, T. Kakeshita, H. Eisaki, and S. Uchida, Phys. Rev. Lett. **109**, 217003 (2012).
[11] A. Dusza, A. Lucarelli, F. Pfuner, J. H. Chu, I. R. Fisher, and L. Degiorgi, Europhys. Lett. **93**, 37 002 (2011).
[12] S. Kasahara, H. J. Shi, K. Hashimoto, S. Tonegawa, Y. Mitzukami, T. Shibauchi, K. Sugimoto, T. Fukuda, T. Terashima, A. H. Nevidomskyy, and Y. Matsuda, Nature (London) **486**, 382 (2012).
[13] R. M. Fernandes, A. V. Chubukov, and J. Schmalian, Nat. Phys. **10**, 97 (2014).
[14] R. M. Fernandes, E. Abrahams, and J. Schmalian, Phys. Rev. Lett. **107**, 217002 (2011).
[15] K. Sugimoto, P. Prelovsek, E. Kaneshita, and T. Tohyama, arXiv:1312.2322.
[16] M. Breitkreiz, P. M. R. Brydon, and C. Timm, arXiv: 1405.5084.
[17] S. Liang, G. Alvarez, C. Şen, A. Moreo, and E. Dagotto, Phys. Rev. Lett. **109**, 047001 (2012).
[18] T.-M. Chuang, M. P. Allan, J. Lee, Y. Xie, N. Ni, S. L. Bud'ko, G. S. Boebinger, P. C. Canfield, and J. C. Davis, Science **327**, 181 (2010).
[19] C.-L. Song, Y.-L. Wang, P. Cheng, Y.-P. Jiang, W. Li, T. Zhang, Z. Li, K. He, L. Wang, J.-F. Jia, H.-H. Hung, C. Wu, X. Ma, X. Chen, and Q.-K. Xue, Science **332**, 1410 (2011).
[20] X. Zhou, C. Ye, P. Cai, X. Wang, X. Chen, and Y. Wang, Phys. Rev. Lett. **106**, 087001 (2011).
[21] S. Grothe, S. Chi, P. Dosanjh, R. Liang, W. N. Hardy, S. A. Burke, D. A. Bonn, and Y. Pennec, Phys. Rev. B **86**, 174503 (2012).
[22] T. Hanaguri (private communication).
[23] M. P. Allan, T.-M. Chuang, F. Massee, Y. Xie, N. Ni, S. L. Bud'ko, G. S. Boebinger, Q. Wang, D. S. Dessau, P. C. Canfield, M. S. Golden, and J. C. Davis, Nat. Phys. **9**, 220 (2013).
[24] E. P. Rosenthal, E. F. Andrade, C. J. Arguello, R. M. Fernandes, L. Y. Xing, X. C. Wang, C. Q. Jin, A. J. Millis, and A. N. Pasupathy, Nat. Phys. **10**, 225 (2014).
[25] J. C. Davis and P. J. Hirschfeld, Nat. Phys. **10**, 184 (2014).
[26] M. N. Gastiasoro, P. J. Hirschfeld, and B. M. Andersen, Phys. Rev. B **89**, 100502(R) (2014).
[27] C.-C. Chen, R. Applegate, B. Moritz, T. P. Devereaux, and R. R. P. Singh, New J. Phys. **13**, 043025 (2011).
[28] Y. Inoue, Y. Yamakawa, and H. Kontani, Phys. Rev. B **85**, 224506 (2012).
[29] N. Plonka, A. F. Kemper, S. Graser, A. P. Kampf, and T. P. Devereaux, Phys. Rev. B **88**, 174518 (2013).
[30] B. M. Andersen, S. Graser, and P. J. Hirschfeld, Europhys. Lett. **97**, 47 002 (2012).
[31] X. Lu, J. T. Park, R. Zhang, H. Luo, A. H. Nevidomskyy, Q. Si, and P. Dai, Science **345**, 657 (2014).
[32] H. Ikeda, R. Arita, and J. Kunes, Phys. Rev. B **81**, 054502 (2010).
[33] B. M. Andersen, P. J. Hirschfeld, A. P. Kampf, and M. Schmid, Phys. Rev. Lett. **99**, 147002 (2007).
[34] M. N. Gastiasoro, P. J. Hirschfeld, and B. M. Andersen, Phys. Rev. B **88**, 220509(R) (2013).
[35] J. M. Ziman, Adv. Phys. **10**, 1 (1961).
[36] W. E. Lawrence and L. A. Cole, J. Phys. F **15**, 883 (1985).
[37] C.-C. Chen, J. Maciejko, A. P. Sorini, B. Moritz, R. R. P. Singh, and T. P. Devereaux, Phys. Rev. B **82**, 100504(R) (2010).
[38] The ratio $(\langle v_x^2\rangle - \langle v_y^2\rangle)/\langle v_x^2\rangle$ is of order 10% for the parameters shown in Fig. 3.
[39] A. E. Böhmer, P. Burger, F. Hardy, T. Wolf, P. Schweiss, R. Fromknecht, M. Reinecker, W. Schranz, and C. Meingast, Phys. Rev. Lett. **112**, 047001 (2014).